The Journal of Cell Biology

Distinct roles of MLCK and ROCK in the regulation of membrane protrusions and focal adhesion dynamics during cell migration of fibroblasts

Go Totsukawa,[1] Yue Wu,[2] Yasuharu Sasaki,[3] David J. Hartshorne,[2] Yoshihiko Yamakita,[1] Shigeko Yamashiro,[1] and Fumio Matsumura[1]

[1]Department of Molecular Biology and Biochemistry, Rutgers University, Piscataway, NJ 08855
[2]Muscle Biology Group, University of Arizona, Tucson, AZ 85721
[3]Department of Pharmacology, School of Pharmaceutical Science, Kitasato University, Tokyo 108-8641, Japan

We examined the role of regulatory myosin light chain (MLC) phosphorylation of myosin II in cell migration of fibroblasts. Myosin light chain kinase (MLCK) inhibition blocked MLC phosphorylation at the cell periphery, but not in the center. MLCK-inhibited cells did not assemble zyxin-containing adhesions at the periphery, but maintained focal adhesions in the center. They generated membrane protrusions all around the cell, turned more frequently, and migrated less effectively. In contrast, Rho-associated kinase (ROCK) inhibition blocked MLC phosphorylation in the center, but not at the periphery.

ROCK-inhibited cells assembled zyxin-containing adhesions at the periphery, but not focal adhesions in the center. They moved faster and more straight. On the other hand, inhibition of myosin phosphatase increased MLC phosphorylation and blocked peripheral membrane ruffling, as well as turnover of focal adhesions and cell migration. Our results suggest that myosin II activated by MLCK at the cell periphery controls membrane ruffling, and that the spatial regulation of MLC phosphorylation plays critical roles in controlling cell migration of fibroblasts.

Introduction

Cell migration is critical for a variety of biological processes in normal and pathological conditions including cellular development, tissue repair, and cancer metastasis. It is a complex process involving a variety of cytoskeletal constituents (Lauffenburger and Horwitz, 1996; Mitchison and Cramer, 1996; Ridley, 2001). The first step of cell migration is the generation of a membrane protrusion in the direction of movement. This process is driven by actin polymerization (Pollard et al., 2000), and may also require the addition of new membrane at the protrusion site. The second step is the establishment of new adhesion sites in the extended membrane. Motile cells assemble transient adhesions at the leading edge, called focal complexes (Nobes and Hall, 1995). In fibroblasts, focal complexes mature into more stable adhesions called focal adhesions (Rottner et al., 1999). Finally,

a contractile force drives the cell body forward, and the rear part of the cell is detached from the substrate.

Myosin II is believed to be involved in the generation of the contractile force for cell migration. The activity of myosin II is mainly controlled by its light chain (MLC) phosphorylation, which is regulated by two classes of enzymes, MLC kinases and myosin phosphatase (Hartshorne et al., 1998; Kamm and Stull, 2001; Somlyo and Somlyo, 2003). Myosin light chain kinase (MLCK) and ROCK/ROK/Rho kinase (called ROCK in this paper) appear to be two major kinases that phosphorylate MLC in vitro as well as in vivo. Other kinases including DAPK (Jin et al., 2001), PAK (Chew et al., 1998), ZIP-kinase (Murata-Hori et al., 1999), and citron kinase (Yamashiro et al., 2003) have been reported to phosphorylate MLC, although the physiological significance is yet to be established. Myosin phosphatase consists of a catalytic subunit of PP1c-delta, a large subunit termed the myosin phosphatase targeting subunit (MYPT, also called MBS or M130) and a 20-kD small subunit (Alessi et

---

al., 1992). MYPT is a major regulator of myosin phosphatase activity because it binds both PP1c and the substrate, phosphorylated myosin II, thus targeting the substrate to the catalytic subunit. MYPT is phosphorylated by a number of kinases including ROCK/ROK/Rho-kinase (Kimura et al., 1996), ZIP-like kinase (MacDonald et al., 2001), integrin-linked kinase (Kiss et al., 2002), myotonic dystrophy protein kinase (Muranyi et al., 2001), and PAK (Takizawa et al., 2002), which results in the inhibition of myosin phosphatase activity. Involvement of other kinases including PKA (Ito et al., 1997), PKG (Surks et al., 1999), and an unidentified mitotic kinase (Totsukawa et al., 1999) in the regulation of myosin phosphatase activity are also suggested.

It is generally accepted that myosin II plays a role in the last step of cell migration, i.e., the translocation of cell body forward by the contraction of the posterior region (Lauffenburger and Horwitz, 1996; Mitchison and Cramer, 1996). This notion is supported by the localization of phosphorylated myosin II at the rear of migrating cells (Post et al., 1995; Matsumura et al., 1998). However, myosin II is likely to play additional and more complex roles in cell migration. Using a specific antibody against phosphorylated MLC, we observed that phosphorylated myosin II is also localized in the anterior regions of motile fibroblasts (Matsumura et al., 1998). Although this observation suggests a role of myosin II other than in rear contraction, little is known about the role of MLC phosphorylation in cell migration at the periphery of the cell.

Using a newly-developed inhibitor of MLCK (Wu et al., 2003) and a well-established inhibitor of ROCK (Uehata et al., 1997), we have been able to block MLC phosphorylation specifically at the periphery and at the cell center, respectively. We found that the spatially-differentiated reduction of MLC phosphorylation produced strikingly opposing effects on the cell migration, as well as on membrane protrusions and the dynamics of focal adhesions of free-moving fibroblasts. Our results indicate new localization-specific roles of phosphorylated myosin II in the regulation of membrane protrusions and cell migration.

Results

Inhibition of MLCK induces multiple membrane protrusions, whereas inhibition of ROCK restricts membrane protrusions mostly to one site

We examined how the inhibition of MLCK or ROCK affects cell migration of free-moving fibroblasts. To block MLCK, we used a new, membrane-permeable biotin-TAT inhibitor (BATI; see Materials and methods). To block ROCK, we used Y-27632, a specific inhibitor of ROCK.

Gerbil fibroma cells were treated with each inhibitor for 30 min, and then cell migration was examined by phase-contrast, time-lapse microscopy (see Videos 1–4, available at http://www.jcb.org/cgi/content/full/jcb.200306172/DC1). Fig. 1 A depicts the images taken at 0 and 60 min from the time-lapse movies (a and b for control; d and e for MLCK-inhibited; g and h for ROCK-inhibited; j and k for both MLCK- and ROCK-inhibited cells). To show net cell translocation, the geographical centers of each cell at 0 (shown in red) and 60 min (black) were determined, and the distance
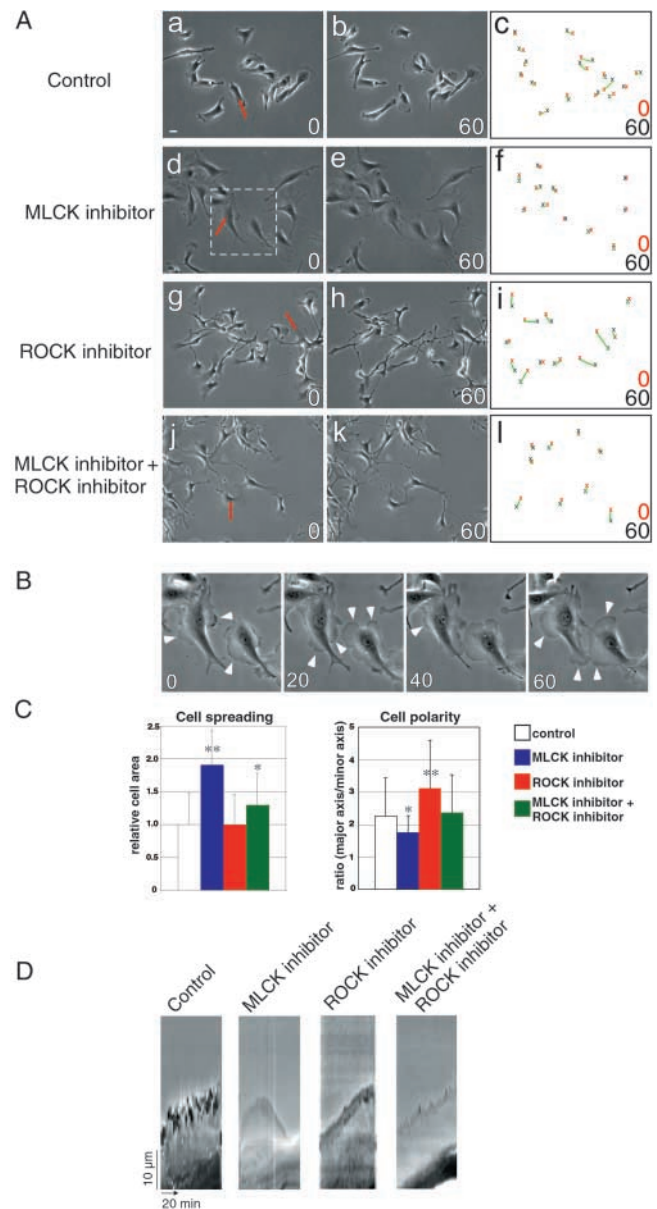
Figure 1.   **Effects of MLCK and ROCK inhibitors on cell migration, membrane protrusions, and cell morphology.** (A) Phase-contrast, time-lapse video microscopy. The left and middle panels of each row show the images at 0 and 60 min, respectively. The right panels of each row show the net translocation (see Results for details). Bar, 20 μm. (B) Multiple protrusions (arrowheads) shown by MLCK-inhibited cells. The time-lapse images at 0, 20, 40, and 60 min correspond to the rectangular portion of A (d). (C) Cell spreading and polarity. Areas of cells and ratios of major and minor axis were measured to determine cell spreading and polarity. *, P < 0.05; **, P < 0.01 as compared with control, t test. (D) Kymograph analyses of membrane protrusions. Red lines (1 pixel wide, 100 pixels long) indicated in A were used for kymograph analyses. At least eight kymograph analyses were performed for each condition. See also Videos 1–4, available at http://www.jcb.org/cgi/content/full/jcb.200306172/DC1.

of migration was shown in c, f, i, and l by connecting two centers. This analysis shows that the inhibition of MLCK reduced net translocation (f). In contrast, the inhibition of ROCK increased translocation of the geographical center (i), though long tails, a characteristic morphology induced by

ROCK inhibition, often remained tethered to the substrate. When both MLCK and ROCK were inhibited, net translocation was similar to that of control cells (compare c with l).

The MLCK and ROCK inhibitors yielded very different effects on cellular morphology, as well as on cell polarity. Although many control cells (Fig. 1 A, a and b; see Video 1) showed polarized morphology with one or two membrane protrusions, MLCK-inhibited cells (Fig. 1 A, d and e; see Video 2) exhibited multiple and broad protrusions all around the cells, resulting in a more spread morphology than control. These protrusions extended and retracted frequently, as shown in Fig. 1 B (arrowheads). In contrast, ROCK-inhibited cells showed one major protrusion and a polarized morphology (Fig. 1 A, g and h; see Video 3). These differences in cell spreading and polarity were confirmed by measurements of cell areas and the ratios of long and short axes, respectively (Fig. 1 C). The average area of MLCK-inhibited cells was 91% larger ($n = 26$) than that of control cells ($n = 64$; P < 0.01, t test), whereas the area of ROCK-inhibited cells ($n = 23$) was very similar to that of control. The area of MLCK- and ROCK-inhibited ($n = 29$) cells was 30% larger than control (P < 0.05, t test). The measurement of cell polarity revealed that ROCK inhibition increased the average ratio by 38% (P < 0.01, t test), whereas MLCK inhibition reduced it by 23% (P < 0.05, t test). The ratio of MLCK- and ROCK-inhibited cells was similar to that of control cells.

Kymograph analyses were performed to examine the effect of MLCK or ROCK inhibition on activity of protrusive membranes (Fig. 1 D). In control cells, the edge of the protrusive membrane was rough, and the phase density of the edge fluctuated greatly, indicating that membranes were dynamically extending and retracting. During the 60-min period, the edge in most control cells moved forward. When MLCK was inhibited, the edge of the membrane was smooth and the phase density of the edge remained relatively low, indicating that membranes did not show cycles of extension and retraction. The movement of the edge was reversed every 10–20 min, resulting in little net translocation of the edge. In contrast, the phase density of the edge of ROCK-inhibited cells is higher than that of MLCK-inhibited cells, but lower than that of control, suggesting that membrane ruffling occurred to a lesser extent than that of control. Most notably, the edge moved forward more consistently and faster than control cells. When both MLCK and ROCK were inhibited, the speed and consistency of forward movement of the membrane edge were similar to those of control cells. However, the phase density of the edge indicates that membrane activity was between those of ROCK- and MLCK-inhibited cells.

MLCK-inhibited cells induced more turns in cell migration, whereas ROCK-inhibited cells moved faster and more straight

To examine in detail the effects of these inhibitors on cell migration, we traced the tracks of migration shown by control, MLCK-inhibited, ROCK-inhibited, and MLCK- and ROCK-inhibited cells (Fig. 2 A). The analyses clearly demonstrated that MLCK-inhibited cells (top right) showed much shorter net translocation than did control cells (top

left). This effect is specific to MLCK inhibition because a peptide containing the TAT vector sequence alone (without the pseudosubstrate sequence of MLCK) showed no effects on cell migration (Fig. S1, available at http://www.jcb. org/cgi/content/full/jcb.200306172/DC1). In contrast to MLCK-inhibited cells, ROCK-inhibited cells (bottom left) traveled much longer distances than did control cells. When both MLCK and ROCK were inhibited (bottom right), the tracks were similar to those of control cells.

The analyses appear to show that MLCK-inhibited cells made turns much more frequently, whereas ROCK-inhibited cells migrated more straight. To confirm this notion, we measured absolute turn angles of trajectory of each segment in these tracks, which is shown in Fig. 2 B as semi-circular histograms. For comparison, the angular distribution of control cells is shown in the right-hand side of each panel. This analysis clearly indicates that MLCK-inhibited cells showed evenly distributed turn angles resulting in random movement (left). In contrast, ROCK-inhibited cells showed more directional migration (middle). When both MLCK and ROCK were inhibited (right), the angular distribution was similar to that of control cells.

Fig. 2 C shows the rates of cell migration, as well as the distances of net translocation during 60-min time periods and directional persistence. These analyses revealed that ROCK-inhibited cells migrated at a considerably higher rate (0.44 ± 0.09 μm/min) than did control cells (0.31 ± 0.04 μm/min; P < 0.01, t test). The higher rate, as well as the lower frequency of turns (Fig. 2 B), explains why ROCK-inhibited cells traveled nearly three times the distance (20.8 ± 5.9 μm) than did control cells (7.6 ± 2.6 μm), and showed the highest directional persistence (0.83 ± 0.14). On the other hand, the net translocation of MLCK-inhibited cells (3.3 ± 1.4 μm) was significantly lower (34%) than that of control cells (P < 0.01, t test), whereas the rate of migration was statistically similar to that of control cells (0.31 ± 0.08 μm/min). Consistent with these analyses, the directional persistence of MLCK-inhibited cells (0.18 ± 0.08) was much lower than that of control cells (0.52 ± 0.10). The inhibition of cell migration by MLCK inhibition is consistent with previous reports that the inactivation of MLCK resulted in the cessation of cell motility of eosinophil and neutrophil cells (Walker et al., 1998; Eddy et al., 2000). When both were inhibited, the rate (0.34 ± 0.06 μm/min), as well as the net translocation (8.6 ± 5.2 μm) and the directional persistence (0.43 ± 0.21), appear to be similar to those values of control cells.

Differential roles of MLCK and ROCK in the spatial regulation of MLC phosphorylation, actin organization, and assembly of focal adhesions

To address the mechanisms by which the inhibition of MLCK and ROCK exerts distinct effects on cell migration and cellular polarity, we examined, by ratio imaging, how these inhibitors alter spatial distribution of MLC phosphorylation (Fig. 3 A), and then analyzed how such alterations affect the assembly of focal adhesions and actin organization (Fig. 3 B). For ratio imaging (Fig. 3 A), cells were double stained with an antibody against the heavy chain of myosin (myosin HC; a, d, g, and j) and anti-phos-

Figure 2. **Effects of the inhibition of MLCK and ROCK on cell migration paths, rates, turn angles, and migration distances.** (A) Analyses of migration paths. Top left, control cells; top right, MLCK-inhibited cells; bottom left, ROCK-inhibited cells; and bottom right, MLCK- and ROCK-inhibited cells. (B) Semicircular histograms showing the distributions of turn angles of trajectory (divided into 20° segments between 0° and 180°). Left, MLCK-inhibited cells (blue); middle, ROCK-inhibited cells (red); and right, MLCK- and ROCK-inhibited cells (green). The histogram of control cells (black) is shown on the right side of each panel for comparison. (C) Left, cell migration rates; middle, total migration distance during a 60-min period; and right, directional persistence of cell migration. Data represent mean ± SD from trajectories of at least eight cells. **, P < 0.01 as compared with control, *t* test.
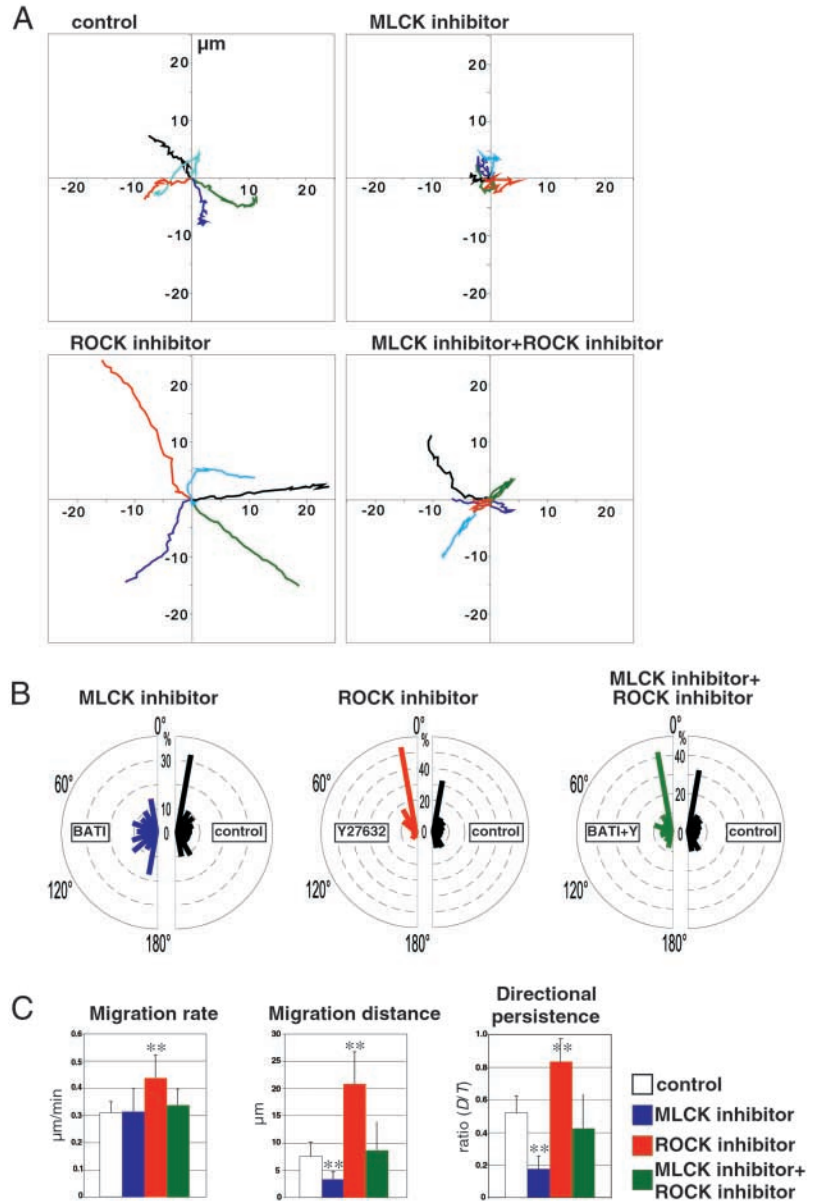

phorylated MLC antibody (P-MLC; b, e, h, and k). Then, ratio images of phosphorylated MLC/total myosin (c, f, i, and l) were generated using IPLab image analysis software (Scanalytics). To examine the organization of focal adhesions and the actin cytoskeleton (Fig. 3 B), cells were triple stained with antibodies against phosphorylated MLC (a, d, g, and j) and vinculin (b, e, h, and k), and with fluorescent phalloidin (c, f, i, and l).

MLCK and ROCK have distinct roles in the spatial regulation of MLC phosphorylation (Fig. 3 A). Control cells (a–c) showed MLC phosphorylation in the center as well as at the periphery (b), as shown previously (Matsumura et al., 1998). Ratio imaging (c) exhibits a bimodal distribution of phosphorylated myosin (arrowhead at the anterior and arrow at the rear). Inhibition of MLCK with BATI greatly reduced MLC phosphorylation specifically at the periphery, but not at the center of the cell (f, cell boundaries indicated by dashed lines). In contrast, ROCK-inhibited cells retained MLC phosphorylation at the anterior re-

gion (h and i, arrowheads), whereas phosphorylation in the center of cells was greatly diminished. Interestingly, ratio imaging (i) revealed the enrichment of phosphorylated myosin at the tail (arrow). When both MLCK and ROCK were blocked, cells showed no enrichment of MLC phosphorylation at either the cell center or periphery (l, arrowheads), verifying the notion that MLCK and ROCK are the major MLC kinases in the cell. Ratio imaging revealed the enrichment of phosphorylated myosin at thin, retraction fiberlike structures (l, arrow).

These alterations in spatial distributions of MLC phosphorylation appear to affect the assembly of adhesive structures and the actin cytoskeleton to a great extent (Fig. 3 B). Control cells showed vinculin staining both in the leading edge and in the center (b), which corresponded to the distribution of phosphorylated MLC in these cells (a). MLCK-inhibited cells (d–f) generated large membrane protrusions around the cells (arrowheads). Concomitant with the specific loss of MLC phosphorylation at these protrusions (d,
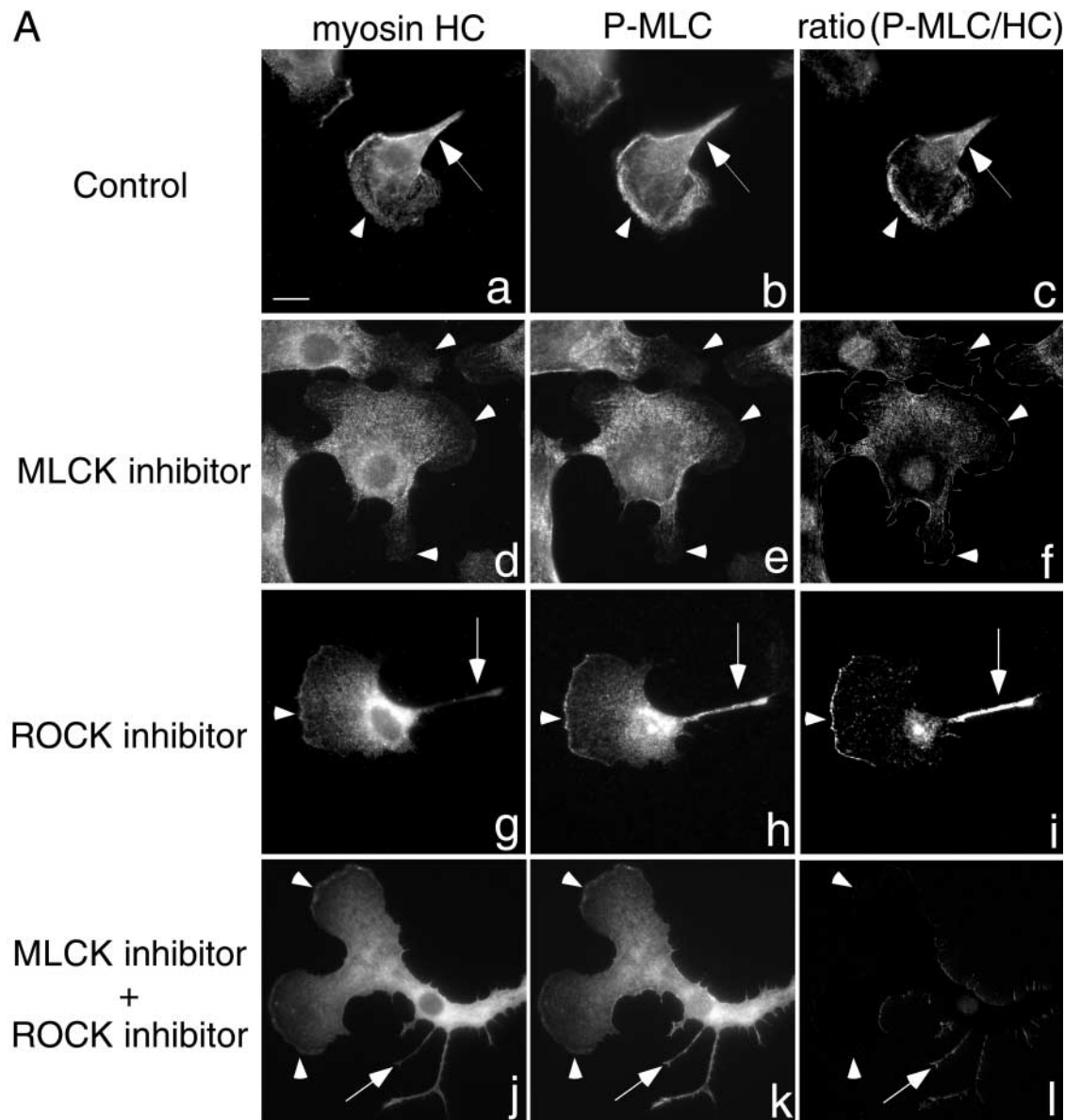
Figure 3.   **Effects of the MLCK and/or ROCK inhibitors on spatial regulation of MLC phosphorylation, as well as on the organization of vinculin and F-actin.** (A) Ratio image analyses of MLC phosphorylation. Control (a–c), MLCK-inhibited (d–f), ROCK-inhibited (g–i), or MLCK- and ROCK-inhibited (j–l) cells were double stained with the antibodies against myosin heavy chain (myosin HC; a, d, g, and j) and phosphorylated MLC (P-MLC; b, e, h, and k). Ratio images of phosphorylated MLC divided by total myosin (P-MLC/HC) are shown in c, f, i, and l. Note that the cell boundaries of MLCK-inhibited cells are outlined by dashed lines in f. (B) Immunofluorescence images of phosphorylated MLC, vinculin, and F-actin (stained by phalloidin). Control (a–c), MLCK-inhibited (d–f), ROCK-inhibited (g–i), or MLCK- and ROCK-inhibited (j–l) cells were triple-stained with antibodies against phosphorylated MLC (P-MLC; a, d, g, and j), vinculin (b, e, h, and k), and with fluorescent phalloidin (c, f, i, and l). Note that the cell boundaries of MLCK-inhibited cells are outlined by dashed lines in d. Bars, 20 μm.

cell boundaries indicated by dashed lines), vinculin staining at this location (e, arrowheads) became much weaker than the control. In contrast, focal adhesions (as well as stress fibers) in the center of cells appeared intact (e and f).

ROCK inhibition produced very different effects (g–i). Vinculin staining at the cell periphery (h, arrowhead) was retained, whereas vinculin staining in the center was lost (h, asterisk). Although stress fibers were disassembled, peripheral actin organization appeared largely unaffected (i, arrowhead). When both MLCK and ROCK were inhibited (j–l), stress fibers as well as peripheral actin filaments disappeared, probably reflecting to the loss of MLC phosphorylation

at the entire region. Vinculin staining (k) was also lost throughout the cytoplasm, though faint staining, reminiscent of focal complexes, was observed at the very edge of membrane protrusions. This suggests that assembly of these structures may not depend on MLC phosphorylation.

The analyses described above indicate that MLCK, but not ROCK, is responsible for MLC phosphorylation at the periphery. Because MLCK is a dedicated kinase that phosphorylates only MLC, MLC phosphorylation by MLCK is likely to control membrane protrusions as well as the assembly of strong vinculin-positive structures at the edge of membrane protrusions. The presence of active MLCK at the
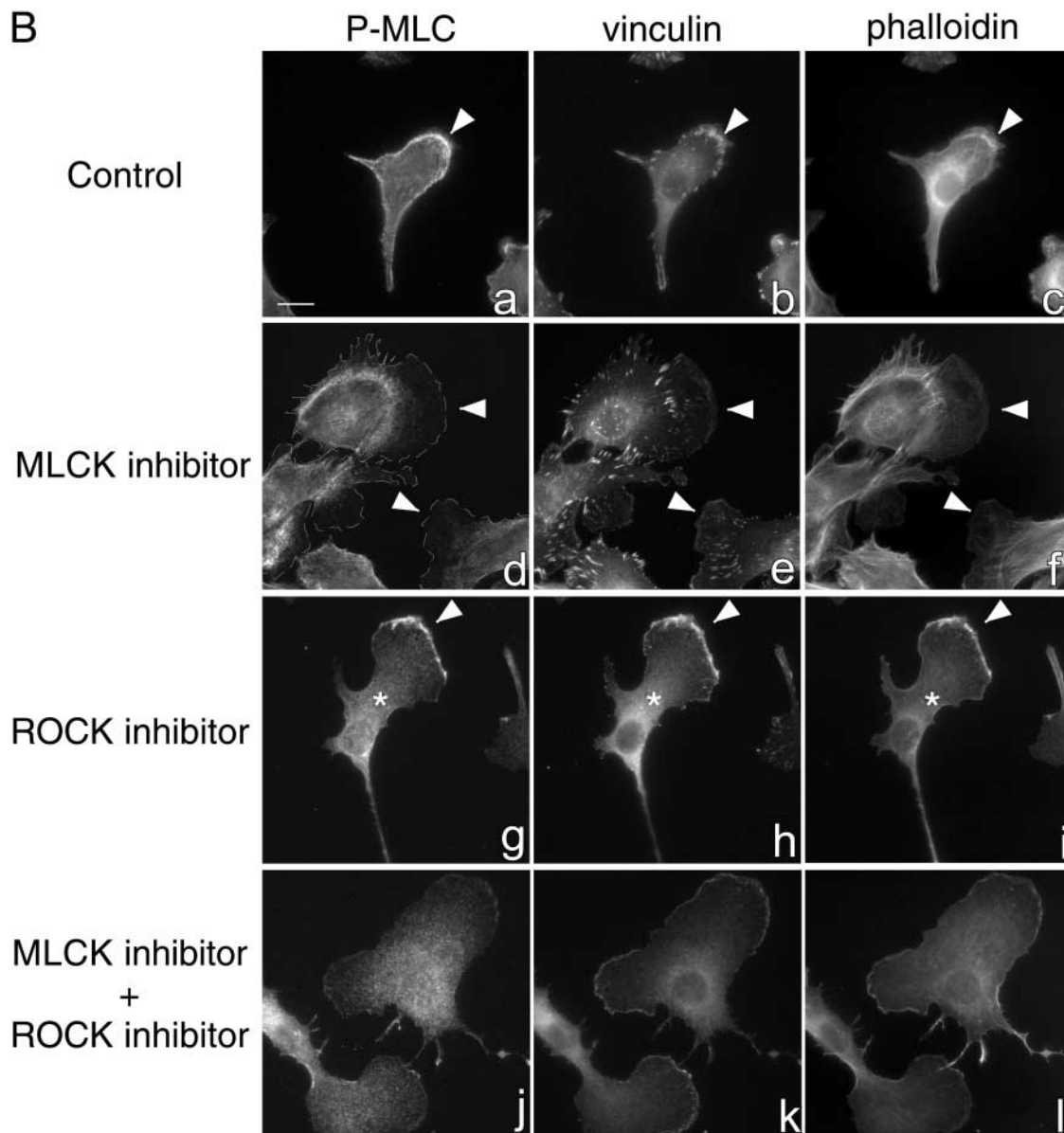
Figure 3 (continued from previous page).

periphery is consistent with FRET analyses, which demonstrated that active MLCK is localized at membrane ruffling (Chew et al., 2002).

Changes in MLC phosphorylation are, at least in part, responsible for the alterations in cell migration and morphology induced by ROCK inhibition

ROCK has been reported to phosphorylate a variety of substrates including MLC, MYPT, ERM proteins, and LIMK (Riento and Ridley, 2003). To determine whether MLC phosphorylation is involved in the ROCK-dependent alterations in cell migration, we examined how expression of a phosphomimetic mutant of MLC (replacing both Ser19 and Thr18 with aspartic acid) modulates cell migration, as well as the organization of actin and focal adhesions of ROCK-inhibited cells. Gerbil fibroma cells were transfected with GFP fusion constructs of the phosphomimetic mutant (MLC-DD) or wild-type MLC (MLC-WT). Transfected cells were then treated with the ROCK inhibitor, and analyzed by time-lapse, phase-contrast microscopy.

We found that expression of the phosphomimetic mutant negated increased cell translocation caused by ROCK inhibition. Fig. 4 A shows GFP fluorescence images for the identification of transfected cells (a and e), as well as phase-contrast images at 0 (b and f) and 60 min (c and g) and the panels showing migration distances during these periods (d and h). Cells expressing MLC-DD (a–d, arrowheads; see also Video 5) exhibited little translocation even in the presence of the ROCK inhibitor, whereas other untransfected cells showed increased migration. In contrast, cells transfected with MLC-WT (e–g, arrowheads) migrated in a way similar to untransfected cells, and frequently showed long tails, a characteristic of ROCK-inhibited cells (e–h, arrowheads; see also Video 6). Analyses of migration tracks (Fig. 4 B) confirmed that cells expressing MLC-DD did not migrate, whereas cells expressing MLC-WT migrated more
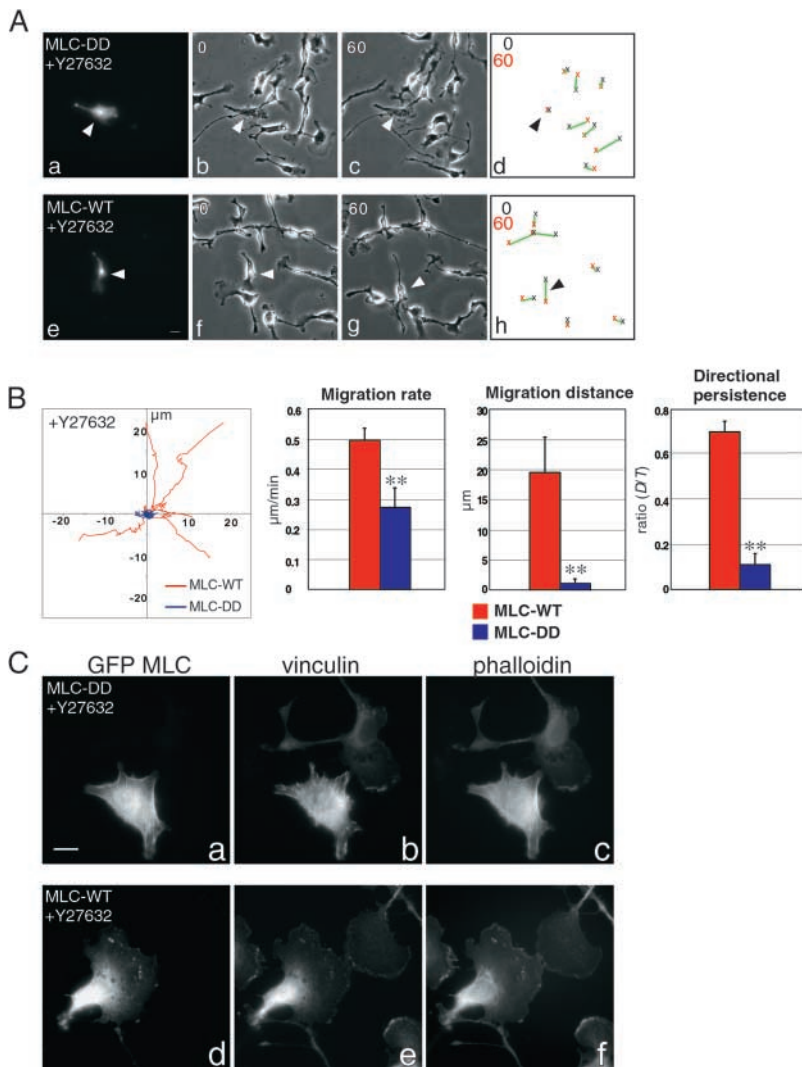
Figure 4. **MLC-DD negated the increased cell translocation caused by ROCK-inhibition.** (A) Cell migration of MLC-DD–expressing cell (a–d, arrowheads) or MLC-WT–expressing cell (e–h, arrowheads) in the presence of the ROCK inhibitor. a and e, GFP fluorescence images. Phase-contrast images were taken at 0 (b and f) and 60 min (c and g). d and h; net translocation during this period. Bar, 20 μm. (B) Migration trajectories (red lines, MLC-WT–expressing cells; blue lines, MLC-DD–expressing cells), migration rates, migration distances, and directional persistence. Data represent mean ± SD from trajectories of at least eight transfected cells. **, P < 0.01, t test. (C) Immunofluorescence images of MLC-DD–expressing cells (a–c) and MLC-WT–expressing cells (d–f). a and d, GFP fluorescence; b and e, vinculin; c and f, phalloidin. Bar, 20 μm. See also Videos 5 and 6, available at http://www.jcb.org/cgi/content/full/jcb.200306172/DC1.

straight and traveled long distances, the pattern of which is indistinguishable from that of untransfected cells (compare Fig. 4 B with Fig. 2 A). The migration rate (0.27 ± 0.06 μm/min) of MLC-DD–expressing cells was decreased to 55% of that (0.49 ± 0.04 μm/min) of cells transfected with MLC-WT, though the reduced rate is similar to that shown by control cells in the absence of ROCK inhibitor (compare Fig. 4 B with Fig. 2 C). The migration distance and directional persistence of MLC-DD–expressing cells were greatly reduced to 1.01 ± 0.65 μm and 0.11 ± 0.04, respectively (those values for MLC-WT–expressing cells were 19.5 ± 5.83 μm and 0.69 ± 0.05, respectively).

As shown in Fig. 4 C, cells expressing MLC-DD retained stress fibers (c) and focal adhesions (b) in the presence of the ROCK inhibitor. In addition, MLC-DD was localized in stress fibers (a). In contrast, cells expressing MLC-WT were similar to untransfected cells. MLC-WT was diffusely present in the cytoplasm (d), and there was no induction of focal adhesions (e) or stress fibers (f). These analyses suggest that the changes in MLC phosphorylation are, at least in part, responsible for the ROCK-dependent alterations in cell migration and cell morphology, though it is possible that changes in phosphorylation

of other ROCK substrates may also be involved in the alterations in cell motility.

ROCK inhibition does not induce Rac activation in gerbil fibroma cells

ROCK inhibition has been reported to activate Rac in Swiss 3T3 cells (Tsuji et al., 2002), and increases membrane ruffling in HUVECs (Wojciak-Stothard and Ridley, 2003). Thus, Rac activation may be a reason for the increased cell motility of gerbil fibroma cells induced by ROCK inhibition. However, a pull-down assay using the GST-PAK-PBD domain revealed that neither ROCK nor MLCK inhibition changed the level of active Rac in our cells (Fig. S2, available at http://www.jcb.org/cgi/content/full/jcb.200306172/DC1).

Inhibition of myosin phosphatase blocked cell migration

The inhibition of cell motility by MLC-DD expression suggests that increased MLC phosphorylation and/or blockage of turnover of MLC phosphorylation inhibit cell migration. To test this idea, we blocked myosin phosphatase by microinjection of a function-inhibiting antibody against MYPT (5 mg/ml) as described previously (Totsukawa et al., 2000), and examined its effects on cell migration, as well as on cel-
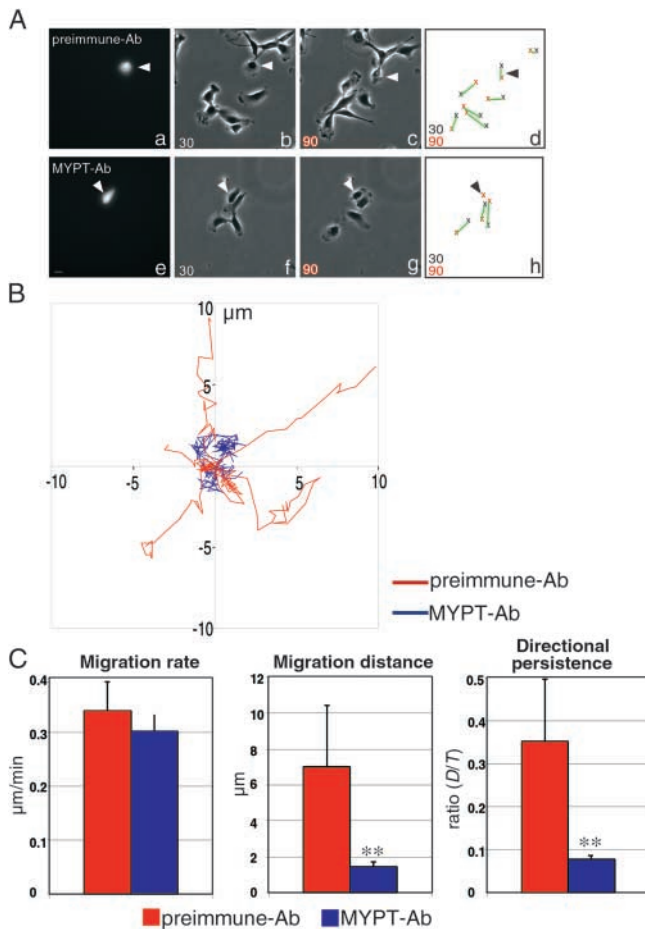
Figure 5. **Inhibition of myosin phosphatase blocks cell migration.**
(A) Cell migration of preimmune-Ab–injected cell (a–d) and MYPT-Ab–injected cell (e–h). Arrowheads denote injected cells. a and e, injection marker. Phase-contrast images were taken at 30 min (b and f) and 90 min (c and g) after microinjection. d and h, net translocation. Bar, 20 μm. (B) Migration paths (red lines for preimmune-Ab and blue lines for MYPT-Ab). (C) Migration rates, migration distances, and directional persistence. Data represent mean ± SD from trajectories of at least eight injected cells. **, P < 0.01, t test. See also Videos 7 and 8, available at http://www.jcb.org/cgi/content/full/jcb.200306172/DC1.

lular morphology and membrane protrusions. As expected, the inhibition of myosin phosphatase greatly increased MLC phosphorylation of gerbil fibroma cells, resulting in thicker stress fibers as well as larger focal adhesions (unpublished data). A preimmune antibody (5 mg/ml) showed no effects on MLC phosphorylation or the organization of the actin cytoskeleton (unpublished data).

Time-lapse, phase-contrast microscopy was performed to analyze effects on cell migration. Fig. 5 A shows the fluorescent images of rhodamine-dextran for an injection marker (a and e); the phase-contrast images captured at 30 (b and f) and 90 min (c and g) after injection, as well as the panels showing migration distances during the 60-min period (d and h). The cell injected with the preimmune-Ab (a–d, indicated by arrowheads; Video 7) migrated as well as other noninjected cells. In contrast, the cell injected with MYPT-Ab (e–h, indicated by arrowheads; Video 8) did not move. The analyses of migration tracks (Fig. 5 B) also revealed that the function-inhibiting antibody blocked

cell migration, whereas the preimmune-Ab showed no significant effect (compare Fig. 5 B with Fig. 2 A, top left). The injection of MYPT-Ab significantly reduced the migration distances and directional persistence to 1.42 ± 0.23 μm (20%) and 0.08 ± 0.01 (22%), respectively, whereas the rate of migration appeared unchanged (Fig. 5 C). In contrast, cells injected with preimmune-Ab showed the migration distance (7.00 μm ± 3.43) and directional persistence (0.35 ± 0.15), similar to those of uninjected cells (compare Fig. 5 C with Fig. 2 C).

MLCK, but not ROCK, is critical for the dynamic assembly of zyxin-containing adhesion structures at the leading edge

Cell migration requires new assembly of attachment sites. Because the MLCK and ROCK inhibitors caused distinct effects on the spatial organization of vinculin-containing structures (Fig. 3 B) as well as motility (Fig. 1 and Fig. 2), we analyzed how these inhibitors affected the dynamics of adhesive structures. To this end, we used cells expressing GFP-zyxin because zyxin is an excellent marker for the assembly of focal complexes, as well as for mature focal adhesions (Rottner et al., 2001). Gerbil fibroma cells were first transfected with GFP-zyxin, treated with the inhibitors, and then observed by time-lapse fluorescence microscopy. Fig. 6 depicts representative images taken from the time-lapse movies.

In control cells, the assembly of focal complexes and adhesions is dynamic (Fig. 6 A, a; Video 9): zyxin-containing structures were newly formed at the periphery of the leading edge. These structures were highly transient (a, arrowheads), and some of them matured into focal adhesions. As reported previously (Smilenov et al., 1999), focal adhesions did not change their positions during cell migration. As the cell moved forward, focal adhesions were located inside the cell and disappeared (most focal adhesions were disassembled within 10 min; see Video 9).

Inhibition of MLCK blocked the formation and/or maturation of zyxin-containing structures at the edge of membrane protrusions (Fig. 6 A, b; Video 10). Although cells produced membrane protrusions all around the cell, these protrusions showed very weak signals of GFP-zyxin (b, arrowheads). On the other hand, many focal adhesions were observed inside the cell and were relatively stable. These observations suggest that MLCK is required for the assembly and/or maturation of zyxin-containing adhesion structures at the leading edge, but not for the assembly of mature focal adhesions in the center.

In contrast, ROCK-inhibited cells (Fig. 6 A, c) assembled highly dynamic zyxin-containing structures at the leading edge (c, arrowheads; Video 11). However, these structures did not mature into focal adhesions as the cell moved forward. Instead, they quickly disassembled inside the cell, indicating that ROCK activity in the center is essential for the maturation into focal adhesions. When both MLCK and ROCK were inhibited (Fig. 6 A, d; Video 12), strong zyxin-positive structures were neither formed at the leading edges nor inside cells. Instead, weak zyxin-containing structures were present as transient small foci all over the cells.
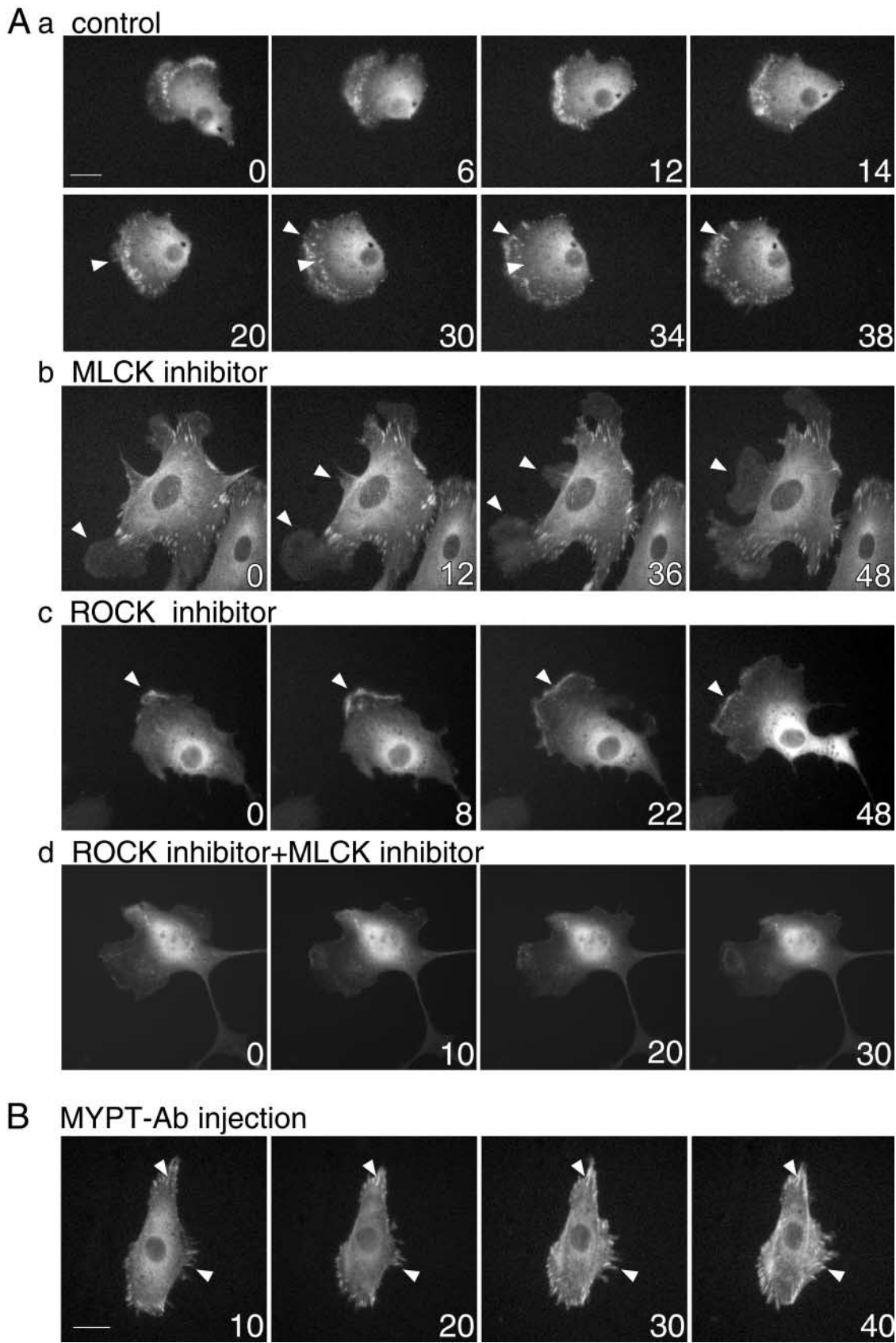
Figure 6.   **Distinct roles of MLCK, ROCK, and myosin phosphatase in the dynamics of zyxin-containing structures.** (A) Time-lapse fluorescence microscopy to examine effects of MLCK and ROCK inhibition. (a) control cells; (b) MLCK-inhibited cells; (c) ROCK-inhibited cells; (d) MLCK- and ROCK-inhibited cells. Times shown in min. (B) Effect of the inhibition of myosin phosphatase. Times after microinjection shown in min. Arrowheads indicate GFP-zyxin–containing structures. Bars, 20 μm. See also Videos 9–13, available at http://www.jcb.org/cgi/content/full/jcb.200306172/DC1.

Inhibition of myosin phosphatase blocked the turnover of focal adhesion assembly

Finally, we examined how the increase in MLC phosphorylation alters the dynamics of focal adhesion assembly. The function-inhibiting antibody was injected into cells expressing GFP-zyxin, and the dynamics of focal adhesion assembly was monitored as described in the previous section.

Injection of the antibody blocked the disassembly of focal adhesions (Fig. 6 B). Although the injected cell initially showed moderate contraction, focal adhesions became longer and larger, and were not disassembled within a 60-min time window (Fig. 6 B, arrowheads; Video 13). In contrast, most focal adhesions of cells injected with the preimmune-Ab disassembled within 10 min (unpublished data). These results indicate that blockage of myosin phosphatase inhibits turnover of focal adhesions, resulting in an inhibition of cell migration. During the initial contraction, the injected cells showed no typical membrane protrusions or ruffling. The contraction eventually stopped ~20–30 min after injection, and then the antibody-injected cell exhibited atypical membrane protrusions (i.e., a burst of short pseudopod-like protrusions; see Video 13). These protrusions quickly retracted, probably due to the high activity of myosin II-based contractility, and no stable zyxin-containing adhesions were established at the protrusions.

Discussion

Localization-specific roles of MLC phosphorylation in cell migration

Our results have elucidated localization-specific roles of myosin II in the regulation of membrane protrusions, as well as in the dynamics of adhesive structures.

Cell periphery and leading edge

We propose that myosin II phosphorylated at the periphery has two functions. First, phosphorylated myosin II at this location restricts membrane protrusions by counteracting protrusive activity powered by actin polymerization. This notion is supported by the observation that the loss of MLC phosphorylation at the periphery of MLCK-inhibited cells resulted in the generation of membrane protrusions all around the cell (Fig. 1 and Fig. 3). It is also supported by the reciprocal experiment: increased MLC phosphorylation as a result of blocking myosin phosphatase inhibited membrane ruffling (Fig. 5). This role for myosin II is also consistent with a previous report showing that a *Dictyostelium* mutant deficient in myosin II extends membrane protrusions in multiple directions (Wessels and Soll, 1990).

Second, phosphorylated myosin II at the periphery is necessary for the assembly and/or maturation of vinculin- and zyxin-containing adhesive structures at the leading edge of motile cells. Although MLCK-inhibited cells formed tiny focal contact-like structures at the very ends of protrusions (Fig. 3 B, e; Fig. 6 A, b), these structures were not assembled or matured into larger adhesions. In addition, the protrusions of MLCK-inhibited cells retracted more frequently than did those of control cells (Fig. 1 D, compare Video 1 with Video 2). These observations suggest that the assembly of and/or maturation into the large vinculin- and zyxin-containing structures provide adhesive sites, thereby stabilizing the membrane protrusion at the anterior part of motile cells. The instability of the protrusions of MLCK-inhibited cells, as well as their occurrence at multiple locations, explains why these cells showed more frequent turns and less efficient cell migration. Though phosphorylated myosin may directly affect the formation of membrane protrusions or adhesions, such effects could also be indirect. For example, MLC phosphorylation may modulate "inside-out" signaling, affecting integrin–ECM interactions, which in turn leads to the alterations in cell protrusions and cell migration.

Cell center

MLC phosphorylation at the center is necessary for the maturation of peripheral adhesive structures into focal adhesions. Vinculin- and zyxin-containing structures assembled at the periphery of ROCK-inhibited cells quickly disappeared without maturing into focal adhesions when they entered into the center (Fig. 6 A, c). Mature focal adhesions are relatively stable structures and probably function as a "brake" on the cell migration machinery. The lack of the brake in ROCK-inhibited cells could explain why these cells moved faster and more straight (Fig. 2), though it is possible that changes in other ROCK substrates may contribute to the alterations in cell migration.

MLCK and ROCK differentially regulate turnover rates of MLC phosphorylation

We suggest that MLCK and ROCK could differentially regulate the dynamics of adhesive structures in these two locations by regulating turnover rates of MLC phosphorylation. Although both MLCK and ROCK can phosphorylate MLC, the specific activity of MLCK is one or two orders higher than that of ROCK (Amano et al., 1996; Feng et al., 1999). Both MLCK and myosin phosphatase are localized in membrane ruffling (Chew et al., 2002; Smith et al., 2003; unpublished data), and such colocalization at the leading edge would result in a high turnover rate of MLC phosphorylation. Because the assembly of vinculin- and zyxin-containing adhesive structures at the leading edge depends on MLC phosphorylation, the high turnover rate would allow dynamic assembly and disassembly of these structures at the leading edge. On the other hand, in the center of cells ROCK may achieve a slower phosphorylation of MLC, and via the phosphorylation of MYPT, inhibit myosin phosphatase. This would result in a very slow turnover rate of MLC phosphorylation in the cell center, which could reflect the relatively stable nature of focal adhesions.

Mechanism for the regulation of anterior MLC phosphorylation during directional migration

The generation of multiple membrane protrusions in MLCK-inhibited cells suggests that if myosin II is inactivated, actin polymerization and resultant membrane protrusions could occur anywhere at the periphery without external signals. Thus, there must be a mechanism that precisely controls MLC phosphorylation at the cell periphery when motile cells show directional motility. The regulation at the

leading edge is probably complex because the leading edge should have a low MLC phosphorylation state for membrane protrusions, and at the same time a high MLC phosphorylation state for the assembly of adhesive structures. Fig. 7 depicts one possible model. We hypothesize that myosin phosphatase is activated at the leading edge of motile cells (Fig. 7, A and B). This could reflect the activation of Rac at the leading edge (Kraynov et al., 2000; Gardiner et al., 2002). Active Rac has been shown to down-regulate Rho activity (Sander et al., 1999), possibly via the activation of p190RhoGAP, a Rho-GTPase activating protein, which is localized at membrane ruffling (Arthur and Burridge, 2001; Nimnual et al., 2003). This would lead to the inactivation of ROCK, thereby negating inhibitory effects on myosin phosphatase, i.e., an apparent activation.

How could the leading edge have both high and low MLC phosphorylation states? One possibility is that MLCK activity could fluctuate. In a low activity state (Fig. 7 A), MLC phosphorylation is reduced, thus allowing a membrane protrusion. In a high activity state (Fig. 7 B), MLC phosphorylation is transiently increased, assembling new and transient adhesions at the periphery. High MLC phosphorylation may also act as a retracting force. The high myosin phosphatase activity, together with changes in MLCK activity, would promote turnover of MLC phosphorylation at the leading edge, causing cycles of protrusions, adhesions, and retraction for cell migration. If myosin phosphatase is inactivated (Fig. 7 C), then MLC phosphorylation is increased at the periphery, restricting membrane protrusions. At the same time, turnover of phosphorylation is reduced, assembling stable adhesions and blocking cell migration. This situation was experimentally realized by blocking myosin phosphatase with the function-inhibiting antibody (Fig. 5 and Fig. 6 B).

Other upstream molecules are likely to participate in the regulation of myosin phosphatase and MLCK during cell migration. Active Rac, for example, may inhibit MLCK at the leading edge because Rac-activated protein kinase (PAK) has been reported to inhibit MLCK by phosphorylating MLCK (Sanders et al., 1999). Other possible regulatory mechanisms for MLCK include inhibition by PKA (Lamb et al., 1988) and activation by MAPK (Klemke et al., 1997). Myosin phosphatase could be regulated by phosphorylation of MYPT with a number of kinases including ROCK, PAK, ZIP-like kinase, myotonic dystrophy protein kinase, and integrin-linked kinase. Obviously, the regulatory mechanism(s) could be complex, and the activities of MLCK and myosin phosphatase probably vary depending on cell types. Such variations may be one of the reasons for cell type–specific responses to the ROCK inhibitors in cell migration. For example, the ROCK inhibitor Y-27632 has been shown to either promote or inhibit cell migration (Itoh et al., 1999; Nobes and Hall, 1999; Wojciak-Stothard and Ridley, 2003). Most recently, it has been reported that the inhibition of ROCK induced multiple membrane protrusions in leukocytes (Worthylake and Burridge, 2003), which is opposite to the results shown here with gerbil fibroma cells. It is possible that MLCK activity may be lower in leukocytes, and the ROCK inhibitor could eliminate MLC phosphorylation even at the anterior region. If so, this would result in
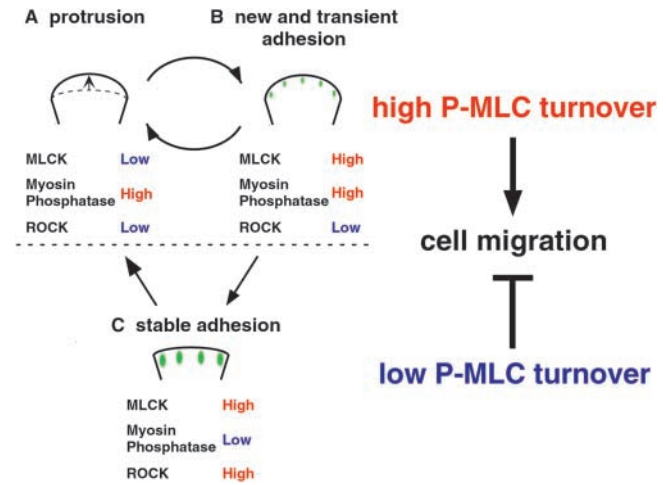
Figure 7. **Model for the role of myosin II phosphorylation at the anterior region of motile cells.** (A) low MLC phosphorylation state at the leading edge of a motile cell; (B) high MLC phosphorylation state at the leading edge of a motile cell; (C) high MLC phosphorylation state at the periphery of a stationary cell. Turnover rates of MLC phosphorylation are high in A and B, but low in C. See Discussion for details.

the generation of multiple protrusions and less efficient cell migration. Future analyses should be directed toward elucidating the upstream signaling cascades that alter the activities of MLCK, ROCK, and myosin phosphatase in different types of cells under specific conditions. It is critical to determine how such alterations result in localization-specific changes in the phosphorylation of MLC, and how spatial alterations in phosphorylation affect cell migration. Such analyses should help us understand how cell motility is regulated in normal and pathological conditions including embryogenesis, tissue repair, and cancer metastasis.

Materials and methods

Reagents, proteins, and antibodies

Antibodies were used as follows: a pAb against MYPT (Totsukawa et al., 2000); an mAb against Ser 19-phosphorylated MLC (Sakurada et al., 1998); a pAb against Ser19-phosphorylated MLC (Matsumura et al., 1998); a pAb against platelet myosin heavy chain (a gift from Drs. J. Sellers and R. Adelstein, National Institutes of Health, Bethesda, MD); an mAb against smooth/nonmuscle myosin heavy chain (Immunotech); a monoclonal anti-Rac1 antibody (BD Biosciences); and a monoclonal anti-vinculin antibody (Sigma-Aldrich).

Y-27632, a specific inhibitor of ROCK, was provided by Yoshitomi Pharmaceutical Industries. A mammalian expression vector for EGFP-zyxin (pEGFP-N1-zyxin) was provided by Drs J. Wehland (Gesellschaft für Biotechnologische Forschung, Braunschweig, Germany) and J.V. Small (Austrian Academy of Sciences, Vienna, Austria); mammalian expression vectors for pEGFP-N1-MLC-WT and pEGFP-N1-MLC-DD were provided by Dr. K. Kelly (National Cancer Institute, Bethesda, MD; Ward et al., 2002); and a bacterial expression vector for GST-PBD was provided by Dr. R.A. Cerione (Cornell University, Ithaca, NY; Bagrodia et al., 1998). Rhodamine-dextran and coumarin-conjugated phalloidin was purchased from Molecular Probes, Inc. and Sigma-Aldrich, respectively.

Membrane-permeable MLCK inhibitor peptide (BATI) was constructed based on the TAT vector and the pseudosubstrate sequence of smooth/nonmuscle MLCK (Wu et al., 2003). The MLCK sequence KKYMARRK-WQKAGHAV (Foster et al., 1990) was fused to the COOH terminus of the TAT sequence YGRKKRRQRRRPPQ (Schwarze et al., 1999); biotin was attached to the NH$_2$ terminus to check membrane permeability. The IC50 for this inhibitor (measured at 1 mM ATP) was 0.4 μM for both smooth muscle and skeletal muscle MLCK (Wu et al., 2003). BATI shows ∼100% transfec-

tion efficiency and is readily transported inside cells within 15 min. BATI showed no inhibition with ROCK. As a control, we used the TAT vector sequence without the pseudosubstrate sequence, which had no inhibitory effect on MLCK activity at 1 mM ATP.

Time-lapse recording

Gerbil fibroma cells (CCL146, American Type Culture Collection) were maintained in DME containing 10% FCS. For time-lapse observation, cells on a coverslip were transferred into Hepes-buffered DME (Invitrogen) containing 10% FCS, and were overlayed with mineral oil to prevent evaporation. Cells were then placed in a temperature control incubator (MS200D, Narishige) to maintain the temperature at 37°C, and were observed under a microscope (TE300; Nikon) with a 20× Plan Fluor phase-contrast (NA 0.45) objective lens. Time-lapse images were taken by a CCD camera (CoolSNAP fx; Roper Scientific) with IPLab image analysis software (Scanalytics). To observe the effects of MLCK or ROCK inhibition, cells were treated with 20 μM BATI and/or 10 μM Y27632 for 30 min before time-lapse recording. Drugs were present during the course of imaging. For the observation of focal adhesion dynamics, cells were microinjected with the expression construct of pEGFP-N1-zyxin. EGFP-zyxin–expressing cells were then processed for time-lapse observation as described above, except that a 40× Plan Fluor phase-contrast lens (NA 0.6) was used. Cells were also transfected with pEGFP-MLC-WT or pEGFP-MLC-DD using LipofectAMINE™ Plus reagent (Invitrogen).

Analysis of cell migration

Motility parameters including rates of migration, migration paths, distances, directional persistence, and kymographs were obtained from time-lapse movies. Images were recorded at 2-min intervals because gerbil fibroma cells seldom changed direction during this time window. To track migration paths, the outlines of individual cells were manually traced for each frame, and the geographical centers were recorded using IPLab image analysis software. The migration paths were expressed as a graph using the Microsoft Excel program. The migration trajectories of at least eight cells were analyzed for each condition. The rates of cell migration were determined by averaging ∼30 segments of migration paths. Migration distances were determined as a net translocation moved during a 60-min period. To visualize the directionality of cell migration, the turn angles made by two consecutive segments of the trajectory was measured, and the distributions of absolute turn angles were shown by a semicircular histogram. Directional persistence (D/T ratio) was calculated as a ratio of the direct distance during a 60-min period (D) and the total length of migration path (T). Cell spreading was determined by measuring cell area, and was expressed as a relative value by normalizing the average area of control cells as 1.0. Cell polarity was determined by measuring a ratio of major and minor axes of the cell. Kymograph analysis of membrane protrusions was performed using IPLab software.

Immunofluorescence

Cells grown on coverslips were fixed with 3.7% formaldehyde in PBS at RT for 10 min, and were permeabilized with acetone at −20°C for 5 min. Primary antibodies used were polyclonal anti-myosin heavy chain (1/500), monoclonal anti-phospho-MLC (1/50), polyclonal anti-phospho-MLC (1/25), or anti-vinculin (1/400). Secondary antibodies used were FITC anti–mouse IgG and TRITC anti–rabbit IgG (1/100, Jackson ImmunoResearch Laboratories). Coumarin-phalloidin was used for F-actin staining. Images were acquired using a microscope (TE300; Nikon) with a 60× (Plan Apo, NA 1.4) phase-contrast objective lens, a CoolSNAP fx CCD camera, and IPLab software. Images were processed using Adobe Photoshop® 6.0. For ratio imaging in Fig. 3, a grayscale image of P-MLC staining (with the mAb) was divided by a corresponding image of total myosin (stained with the pAb to myosin heavy chain) using IPLab software. Essentially, the same results were obtained by ratio imaging using the mAb against myosin heavy chain and the pAb against P-MLC.

Online supplemental material

Fig. S1 shows that the TAT control peptide has no effect on cell morphology and migration. Fig. S2 shows that Rac is not activated by Y27632 or BATI treatment. The corresponding QuickTime movie files of live cells are organized as follows: Videos 1–4 for Fig. 1 A; Videos 5 and 6 for Fig. 4 A; Videos 7 and 8 for Fig. 5 A; Videos 9–12 for Fig. 6 A; and Video 13 for Fig. 6 B. Supplemental material available online at http://www.jcb.org/cgi/content/full/jcb.200306172/DC1.

___

References

Alessi, D., L.K. MacDougall, M.M. Sola, M. Ikebe, and P. Cohen. 1992. The control of protein phosphatase-1 by targetting subunits. The major myosin phosphatase in avian smooth muscle is a novel form of protein phosphatase-1. *Eur. J. Biochem.* 210:1023–1035.

Amano, M., M. Ito, K. Kimura, Y. Fukata, K. Chihara, T. Nakano, Y. Matsuura, and K. Kaibuchi. 1996. Phosphorylation and activation of myosin by Rho-associated kinase (Rho-kinase). *J. Biol. Chem.* 271:20246–20249.

Arthur, W.T., and K. Burridge. 2001. RhoA inactivation by p190RhoGAP regulates cell spreading and migration by promoting membrane protrusion and polarity. *Mol. Biol. Cell.* 12:2711–2720.

Bagrodia, S., S.J. Taylor, K.A. Jordon, L. Van Aelst, and R.A. Cerione. 1998. A novel regulator of p21-activated kinases. *J. Biol. Chem.* 273:23633–23636.

Chew, T.L., R.A. Masaracchia, Z.M. Goeckeler, and R.B. Wysolmerski. 1998. Phosphorylation of non-muscle myosin II regulatory light chain by p21-activated kinase (gamma-PAK). *J. Muscle Res. Cell Motil.* 19:839–854.

Chew, T.L., W.A. Wolf, P.J. Gallagher, F. Matsumura, and R.L. Chisholm. 2002. A fluorescent resonant energy transfer-based biosensor reveals transient and regional myosin light chain kinase activation in lamella and cleavage furrows. *J. Cell Biol.* 156:543–553.

Eddy, R.J., L.M. Pierini, F. Matsumura, and F.R. Maxfield. 2000. Ca²⁺-dependent myosin II activation is required for uropod retraction during neutrophil migration. *J. Cell Sci.* 113:1287–1298.

Feng, J., M. Ito, Y. Kureishi, K. Ichikawa, M. Amano, N. Isaka, K. Okawa, A. Iwamatsu, K. Kaibuchi, D.J. Hartshorne, and T. Nakano. 1999. Rho-associated kinase of chicken gizzard smooth muscle. *J. Biol. Chem.* 274:3744–3752.

Foster, C.J., S.A. Johnston, B. Sunday, and F.C. Gaeta. 1990. Potent peptide inhibitors of smooth muscle myosin light chain kinase: mapping of the pseudosubstrate and calmodulin binding domains. *Arch. Biochem. Biophys.* 280:397–404.

Gardiner, E.M., K.N. Pestonjamasp, B.P. Bohl, C. Chamberlain, K.M. Hahn, and G.M. Bokoch. 2002. Spatial and temporal analysis of Rac activation during live neutrophil chemotaxis. *Curr. Biol.* 12:2029–2034.

Hartshorne, D.J., M. Ito, and F. Erdodi. 1998. Myosin light chain phosphatase: subunit composition, interactions and regulation. *J. Muscle Res. Cell Motil.* 19:325–341.

Ito, M., J. Feng, S. Tsujino, N. Inagaki, M. Inagaki, J. Tanaka, K. Ichikawa, D.J. Hartshorne, and T. Nakano. 1997. Interaction of smooth muscle myosin phosphatase with phospholipids. *Biochemistry.* 36:7607–7614.

Itoh, K., K. Yoshioka, H. Akedo, M. Uehata, T. Ishizaki, and S. Narumiya. 1999. An essential part for Rho-associated kinase in the transcellular invasion of tumor cells. *Nat. Med.* 5:221–225.

Jin, Y., E.K. Blue, S. Dixon, L. Hou, R.B. Wysolmerski, and P.J. Gallagher. 2001. Identification of a new form of death-associated protein kinase that promotes cell survival. *J. Biol. Chem.* 276:39667–39678.

Kamm, K.E., and J.T. Stull. 2001. Dedicated myosin light chain kinases with diverse cellular functions. *J. Biol. Chem.* 276:4527–4530.

Kimura, K., M. Ito, M. Amano, K. Chihara, Y. Fukata, M. Nakafuku, B. Yamamori, J. Feng, T. Nakano, K. Okawa, et al. 1996. Regulation of myosin phosphatase by Rho and Rho-associated kinase (Rho-kinase). *Science.* 273:245–248.

Kiss, E., A. Muranyi, C. Csortos, P. Gergely, M. Ito, D.J. Hartshorne, and F. Erdodi. 2002. Integrin-linked kinase phosphorylates the myosin phosphatase target subunit at the inhibitory site in platelet cytoskeleton. *Biochem. J.* 365:79–87.

Klemke, R.L., S. Cai, A.L. Giannini, P.J. Gallagher, P. de Lanerolle, and D.A. Cheresh. 1997. Regulation of cell motility by mitogen-activated protein kinase. *J. Cell Biol.* 137:481–492.

Kraynov, V.S., C. Chamberlain, G.M. Bokoch, M.A. Schwartz, S. Slabaugh, and K.M. Hahn. 2000. Localized Rac activation dynamics visualized in living cells. *Science.* 290:333–337.

Lamb, N.J., A. Fernandez, M.A. Conti, R. Adelstein, D.B. Glass, W.J. Welch, and J.R. Feramisco. 1988. Regulation of actin microfilament integrity in living nonmuscle cells by the cAMP-dependent protein kinase and the myosin light chain kinase. *J. Cell Biol.* 106:1955–1971.

Lauffenburger, D.A., and A.F. Horwitz. 1996. Cell migration: a physically integrated molecular process. *Cell.* 84:359–369.

MacDonald, J.A., M.A. Borman, A. Muranyi, A.V. Somlyo, D.J. Hartshorne, and T.A. Haystead. 2001. Identification of the endogenous smooth muscle myosin phosphatase-associated kinase. *Proc. Natl. Acad. Sci. USA.* 98:2419–2424.

Matsumura, F., S. Ono, Y. Yamakita, G. Totsukawa, and S. Yamashiro. 1998. Specific localization of serine 19 phosphorylated myosin II during cell locomotion and mitosis of cultured cells. *J. Cell Biol.* 140:119–129.

Mitchison, T.J., and L.P. Cramer. 1996. Actin-based cell motility and cell locomotion. *Cell.* 84:371–379.

Muranyi, A., R. Zhang, F. Liu, K. Hirano, M. Ito, H.F. Epstein, and D.J. Hartshorne. 2001. Myotonic dystrophy protein kinase phosphorylates the myosin phosphatase targeting subunit and inhibits myosin phosphatase activity. *FEBS Lett.* 493:80–84.

Murata-Hori, M., F. Suizu, T. Iwasaki, A. Kikuchi, and H. Hosoya. 1999. ZIP kinase identified as a novel myosin regulatory light chain kinase in HeLa cells. *FEBS Lett.* 451:81–84.

Nimnual, A.S., L.J. Taylor, and D. Bar-Sagi. 2003. Redox-dependent downregulation of Rho by Rac. *Nat. Cell Biol.* 5:236–241.

Nobes, C.D., and A. Hall. 1995. Rho, rac, and cdc42 GTPases regulate the assembly of multimolecular focal complexes associated with actin stress fibers, lamellipodia, and filopodia. *Cell.* 81:53–62.

Nobes, C.D., and A. Hall. 1999. Rho GTPases control polarity, protrusion, and adhesion during cell movement. *J. Cell Biol.* 144:1235–1244.

Pollard, T.D., L. Blanchoin, and R.D. Mullins. 2000. Molecular mechanisms controlling actin filament dynamics in nonmuscle cells. *Annu. Rev. Biophys. Biomol. Struct.* 29:545–576.

Post, P.L., R.L. DeBiasio, and D.L. Taylor. 1995. A fluorescent protein biosensor of myosin II regulatory light chain phosphorylation reports a gradient of phosphorylated myosin II in migrating cells. *Mol. Biol. Cell.* 6:1755–1768.

Ridley, A.J. 2001. Rho GTPases and cell migration. *J. Cell Sci.* 114:2713–2722.

Riento, K., and A.J. Ridley. 2003. Rocks: multifunctional kinases in cell behaviour. *Nat. Rev. Mol. Cell Biol.* 4:446–456.

Rottner, K., A. Hall, and J.V. Small. 1999. Interplay between Rac and Rho in the control of substrate contact dynamics. *Curr. Biol.* 9:640–648.

Rottner, K., M. Krause, M. Gimona, J.V. Small, and J. Wehland. 2001. Zyxin is not colocalized with vasodilator-stimulated phosphoprotein (VASP) at lamellipodial tips and exhibits different dynamics to vinculin, paxillin, and VASP in focal adhesions. *Mol. Biol. Cell.* 12:3103–3113.

Sakurada, K., M. Seto, and Y. Sasaki. 1998. Dynamics of myosin light chain phosphorylation at Ser19 and Thr18/Ser19 in smooth muscle cells in culture. *Am. J. Physiol.* 274:C1563–C1572.

Sander, E.E., J.P. ten Klooster, S. van Delft, R.A. van der Kammen, and J.G. Collard. 1999. Rac downregulates Rho activity: reciprocal balance between both GTPases determines cellular morphology and migratory behavior. *J. Cell Biol.* 147:1009–1022.

Sanders, L.C., F. Matsumura, G.M. Bokoch, and P. de Lanerolle. 1999. Inhibition of myosin light chain kinase by p21-activated kinase. *Science.* 283:2083–2085.

Schwarze, S.R., A. Ho, A. Vocero-Akbani, and S.F. Dowdy. 1999. In vivo protein transduction: delivery of a biologically active protein into the mouse. *Science.* 285:1569–1572.

Smilenov, L.B., A. Mikhailov, R.J. Pelham, E.E. Marcantonio, and G.G. Gundersen. 1999. Focal adhesion motility revealed in stationary fibroblasts. *Science.* 286:1172–1174.

Smith, A., M. Bracke, B. Leitinger, J.C. Porter, and N. Hogg. 2003. LFA-1-induced T cell migration on ICAM-1 involves regulation of MLCK-mediated attachment and ROCK-dependent detachment. *J. Cell Sci.* 116:3123–3133.

Somlyo, A.P., and A.V. Somlyo. 2003. Ca^{2+} sensitivity of smooth muscle and nonmuscle myosin II: modulated by G proteins, kinases, and myosin phosphatase. *Physiol. Rev.* 83:1325–1358.

Surks, H.K., N. Mochizuki, Y. Kasai, S.P. Georgescu, K.M. Tang, M. Ito, T.M. Lincoln, and M.E. Mendelsohn. 1999. Regulation of myosin phosphatase by a specific interaction with cGMP-dependent protein kinase Iα. *Science.* 286:1583–1587.

Takizawa, N., Y. Koga, and M. Ikebe. 2002. Phosphorylation of CPI17 and myosin binding subunit of type 1 protein phosphatase by p21-activated kinase. *Biochem. Biophys. Res. Commun.* 297:773–778.

Totsukawa, G., Y. Yamakita, S. Yamashiro, H. Hosoya, D.J. Hartshorne, and F. Matsumura. 1999. Activation of myosin phosphatase targeting subunit by mitosis-specific phosphorylation. *J. Cell Biol.* 144:735–744.

Totsukawa, G., Y. Yamakita, S. Yamashiro, D.J. Hartshorne, Y. Sasaki, and F. Matsumura. 2000. Distinct roles of ROCK (Rho-kinase) and MLCK in spatial regulation of MLC phosphorylation for assembly of stress fibers and focal adhesions in 3T3 fibroblasts. *J. Cell Biol.* 150:797–806.

Tsuji, T., T. Ishizaki, M. Okamoto, C. Higashida, K. Kimura, T. Furuyashiki, Y. Arakawa, R.B. Birge, T. Nakamoto, H. Hirai, and S. Narumiya. 2002. ROCK and mDia1 antagonize in Rho-dependent Rac activation in Swiss 3T3 fibroblasts. *J. Cell Biol.* 157:819–830.

Uehata, M., T. Ishizaki, H. Satoh, T. Ono, T. Kawahara, T. Morishita, H. Tamakawa, K. Yamagami, J. Inui, M. Maekawa, and S. Narumiya. 1997. Calcium sensitization of smooth muscle mediated by a Rho-associated protein kinase in hypertension. *Nature.* 389:990–994.

Walker, J.W., S.H. Gilbert, R.M. Drummond, M. Yamada, R. Sreekumar, R.E. Carraway, M. Ikebe, and F.S. Fay. 1998. Signaling pathways underlying eosinophil cell motility revealed by using caged peptides. *Proc. Natl. Acad. Sci. USA.* 95:1568–1573.

Ward, Y., S.F. Yap, V. Ravichandran, F. Matsumura, M. Ito, B. Spinelli, and K. Kelly. 2002. The GTP binding proteins Gem and Rad are negative regulators of the Rho-Rho kinase pathway. *J. Cell Biol.* 157:291–302.

Wessels, D., and D.R. Soll. 1990. Myosin II heavy chain null mutant of *Dictyostelium* exhibits defective intracellular particle movement. *J. Cell Biol.* 111:1137–1148.

Wojciak-Stothard, B., and A.J. Ridley. 2003. Shear stress-induced endothelial cell polarization is mediated by Rho and Rac but not Cdc42 or PI 3-kinases. *J. Cell Biol.* 161:429–439.

Worthylake, R.A., and K. Burridge. 2003. RhoA and ROCK promote migration by limiting membrane protrusions. *J. Biol. Chem.* 278:13578–13584.

Wu, Y., F. Erdodi, A. Murányi, K.D. Nullmeyer, R.M. Lynch, and D.J. Hartshorne. 2003. Myosin phosphatase and myosin phosphorylation in differentiating C2C12 cells. *J. Muscle Res. Cell Motil.* 24:499–511.

Yamashiro, S., G. Totsukawa, Y. Yamakita, Y. Sasaki, P. Madaule, T. Ishizaki, S. Narumiya, and F. Matsumura. 2003. Citron kinase, a Rho-dependent kinase, induces di-phosphorylation of regulatory light chain of myosin II. *Mol. Biol. Cell.* 14:1745–1756.